Revisiting Sparsity Hunting in Federated Learning: Why the Sparsity Consensus Matters?

Anonymous authors
Paper under double-blind review

Abstract

Edge devices can benefit remarkably from federated learning due to their distributed nature; however, their limited resource and compute power pose limitations in deployment. A possible solution to this problem is to utilize off-the-shelf sparse learning algorithms at the clients to meet their resource budget. However, such naive deployment causes significant accuracy degradation, especially for highly resource-constrained clients. In particular, our investigations reveal that the lack of consensus in the trained sparsity masks among the clients may potentially lead to slower convergence of the global model, which can further result in a substantial accuracy drop. Based on our observations, we present *federated lottery aware sparsity hunting* (FLASH), a unified sparse learning framework for training a sparse sub-model that maintains the performance under ultra low parameter density while yielding proportional communication benefits. Moreover, given that different clients may have different resource budgets, we further extend our algorithm to present *hetero-FLASH* where instead of supporting only one target parameter density, clients can take different density budgets based on their device resource limitations. Experimental evaluations on diverse models and datasets show the superiority of FLASH in closing the gap with an unpruned baseline while yielding up to ∼10.1% improved accuracy with ∼10.26× fewer communication costs, compared to existing alternatives, at similar hyperparameter settings.

1 Introduction

Federated learning (FL) (McMahan et al., 2017) is a popular form of distributed training, which has gained significant traction due to its ability to allow multiple clients to learn a common global model without sharing their private data. However, clients' heterogeneity and resource limitations pose significant challenges for FL deployment over edge nodes, including mobile and IoT devices. To resolve these issues, various methods have been proposed over the past few years, including efficient learning for heterogeneous collaborative training (Lin et al., 2020; Zhu et al., 2021), distillation (He et al., 2020), federated dropout techniques (Horvath et al., 2021; Caldas et al., 2018b), efficient aggregation for faster convergence and reduced communication (Reddi et al., 2020; Li et al., 2020b). However, these methods do not necessarily address the growing concerns of high computation and communication limited edge.

Meanwhile, reducing the memory, compute, and latency costs for deep neural networks in centralized training for their efficient edge deployment has also become an active area of research. In particular, recently proposed *sparse learning* (SL) strategies (Evci et al., 2020; Kundu et al., 2021b; 2022; Mocanu et al., 2018; Dettmers & Zettlemoyer, 2019) effectively train weights and associated binary *sparse masks* such that only a fraction of model parameters (density $d \ll 1$) are non-zero during training. This enables the potential for reduction in both the training time and compute cost (Qiu et al., 2021; Raihan & Aamodt, 2020), *while yielding accuracy close to that of the unpruned baseline.*

In addition to the aforementioned benefits of sparse learning in centralized settings, its proper deployment in FL can reduce communication costs. In particular, users can train larger models while communicating only a fraction of weights that are non-zero (Fig. 1 (a)). However, the challenges and opportunities of sparse learning in FL are yet to be fully unveiled. Only very recently, few works (Bibikar et al., 2022; Huang et al., 2022) have tried to leverage non-aggressive model compression in FL. Another recent work, ZeroFL (Qiu et al., 2021), has explored deploying sparse learning in FL; however, failed to leverage the advantages of model sparsity to reduce the clients' communication costs. Moreover, as shown in Fig. 1(b), for $d = 0.05$, ZeroFL suffers from a substantial accuracy drop of ∼14% compared to the baseline.

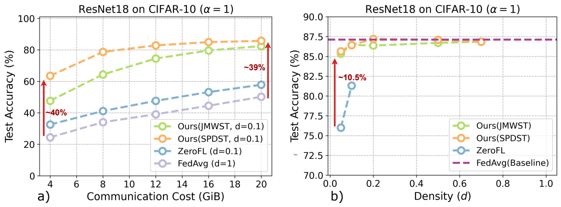

Figure 1: (a) Accuracy vs. Communication. For a given communication threshold, sparse learning in FL can improve performance. (b) Accuracy vs. parameter density in each client. Our approach significantly outperforms the existing alternative (Qiu et al., 2021).

Contributions. Our contribution is fourfold. In view of the above, we first present crucial observations in identifying several limitations in integrating sparse learning in federated settings. In particular, we observe that the sparse aggregated model does not converge to a unique sparsity pattern, primarily due to the **lack of consensus** among the clients' individual masks in different rounds. In contrast, in centralized training, as the model matures, the mask also shows a higher convergence trend. We further empirically demonstrate the utility of incorporating layer importance and clients' consensus on the performance.

We then leverage our findings and present *federated lottery aware sparsity hunting* (FLASH), a methodology that can achieve both computation and communication efficiency in FL by employing sparse learning.

Furthermore, in real-world scenarios, FL users are more likely to have highly *heterogeneous resource budgets* (Diao et al., 2020). Therefore, instead of limiting everyone by the minimum available resource, we extend our methodology to *hetero*-FLASH, where different clients can participate with different sparsity budgets yet yield a sparse model, leveraging the resource and data of each client while adhering to their own resource limit. Here, to deal with this problem, we propose server-side sub-sampling where the server creates multiple sub-masks of the global model's mask such that all follow the global layer importance.

We conduct experiments on MNIST, FEMNIST, CIFAR-10, CIFAR-100, and TinyImageNet with different models for both IID and non-IID client data partitioning. Our results show that compared to the existing alternative (Qiu et al., 2021), at iso-hyperparameter settings, FLASH can yield up to ∼8.9% and ∼10.1%, on IID and non-IID data settings, respectively, with reduced communication of up to ∼10.2×.

2 Related Works

Model Pruning. Over the past few years, a plethora of research has been done to perform efficient model compression via pruning, particularly in centralized training (Frankle & Carbin, 2018; Liu et al., 2021; You et al., 2019; Kundu & Sundaresan, 2021). Pruning essentially identifies and removes the unimportant weights to yield efficient inference models. More recently, sparse learning (Evci et al., 2020; Dettmers & Zettlemoyer, 2019; Kundu et al., 2020; 2019), a popular form of model pruning, has gained significant traction as it can yield FLOPs saving even during training. In particular, it ensures only d% of the model parameters remain non-zero during the training for a target parameter density d ($d << 1.0$ and sparsity is $1.0 - d$). In this way, FL users potentially need to share d% of their updates to the server.

Sparse Learning. We leverage Dettmers & Zettlemoyer (2019) to sparsely learn the sparsity mask of each client. In Dettmers & Zettlemoyer (2019), training starts with a sparse model with a randomly initiated mask meeting the target parameter density d. In particular, since there is no prior knowledge about the importance of weights and layers, we start with a random sparse mask that has uniform layer-wise parameter density d. At the end of each epoch, the mask gets updates based on a *prune-regrow* policy. In specific, first a ranking of the layers are done based on their normalized momentum contribution of the non-zero weights. The model then prunes the lowest p_r%[1] weights from each layer based on their absolute magnitude. As p_r% pruning happens on top of the sparse model with density d, it allows p_r% weights to regrow into locations

---

[1] Prune rate (p_r) indicates the % of weights pruned from each layer of a sparse model.

of masks with zero values, removing $p_r\%$ of non-zeros from the mask. Finally, total $p_r\%$ of weights are regrown where each layer gets number of regrown weights proportional to their normalized layer importance evaluated based on their momentum contribution. This allows layers with high rank/importance to have more non-zero weights. This process iteratively repeats each epoch to finally learn the mask as well as non-zero weights. Note that there are multiple choices for pruning and regrowing the weights; however, we chose absolute magnitude, saving the clients to compute additional values such as the momentum.

FL for resource and communication limited edge. Heterogeneity and limitations of resources, especially for edge devices, are among the most known challenges of cross-device federated learning (Kairouz et al., 2021). Existing works have explored the idea of heterogeneous training that allows heterogeneous clients to train on different fractions of full-model based on their compute budget (Horvath et al., 2021; Diao et al., 2020; Mei et al., 2022). On a parallel track, various optimizations are proposed to accelerate the convergence, thus requiring fewer communication rounds (Han et al., 2020; Gorbunov et al., 2021; Zhang et al., 2013; Li et al., 2019).

To make FL more communication efficient, a few research have leveraged pruning in FL (Li et al., 2020a; Jiang et al., 2022; Li et al., 2021). In LotteryFL (Li et al., 2020a), clients adapt personalized masks that perform well only on their local data. Moreover, the clients need to regularly communicate the entire model to the server. Similarly, PruneFL (Jiang et al., 2022) also asks for high communication costs as it demands the participating clients to send the gradient values of entire model to the server while updating the masks.

Only a few contemporary works (Huang et al., 2022; Bibikar et al., 2022; Qiu et al., 2021) tried to leverage the benefits of sparse learning in federated settings. In particular, Huang et al. (2022) relied on a randomly initialized sparse mask and recommended keeping it frozen throughout the training yet failed to provide any supporting intuition. FedDST (Bibikar et al., 2022), on the other hand, leveraged the idea of RigL (Evci et al., 2020) to perform sparse learning of the clients. It relied on a large number of local epochs to avoid gradient noise and focused primarily on only highly non-IID data without targeting ultra-low density d. More importantly, neither of these works investigated the key differences between centralized and FL sparse learning. With similar philosophy as ours, ZeroFL (Qiu et al., 2021) first identified a fundamental aspect of sparse learning in FL. Then showed that the top-k weights of clients are more likely to differ for low densities; hence the aggregated updates cannot benefit anyone. However, most of the weights are shared in denser updates. Therefore, despite training each client with low density $d = 0.1$, they propose to send updates of a model with $d = 0.3$ of the total model weights to improve accuracy at high compression. Thus, this approach fails to yield proportional communication efficiency as even for a low parameter density d; all clients had to download the full model and send back a 3× denser model while suffering from a significant accuracy drop.

Another contemporary work (Isik et al., 2023) leveraged the idea of learning the sparse mask while keeping the weights fixed to their initialized values (Ramanujan et al., 2020). Thus, clients are only required to send the binary mask updates to the server reducing the communication by 32×. However, due to SGD-based updating of floating point mask for each weight, such methods do not necessarily help the client's local computation. Such an assumption is out of our current scope, as we assume an even stricter constraint where no client can perform dense model updates or storage while yielding significant communication savings.

3 Revisiting Sparse Learning: Why Does it Miss the Mark in FL?

In centralized training applying sparse learning methods has shown benefits within FLOPs reduction during forward operations (Evci et al., 2020), and potential training speed-up of up to 3.3× (Qiu et al., 2021) while maintaining high accuracy at low densities ($d \leq 0.1$). However, here, the primary purpose of employing sparse learning is to utilize communication efficiency by reducing update size in FL. Such methods can potentially get better convergence and performance compared to post-training or data-independent methods.

In this section, we conduct an exhaustive analysis to understand how naive deployment of sparse learning in FL works while unveiling key differentiating factors in training dynamics with sparse learning in centralized to that of FL. We used a widely adopted FL training setting (Qiu et al., 2021; Diao et al., 2020) (refer to Table 1 for details) on the CIFAR-10 dataset and added sparse learning on the clients. Here, each client

Table 1: FL training settings considered in this work.

Dataset	Model	Data-partioning	Rounds (T)	Clients (C_N)	Clients/Round (c_r, c_d)	Optimizer	Aggregation	Local epoch (E)	Batch size
MNIST	MNISTNet	LDA	400	100	10, 10	SGD	FedAvg	1	32
CIFAR-10	ResNet18		600						
CIFAR-100			800						
TinyImageNet			600						
FEMNIST	Same as (Caldas et al., 2018a)	–	1000	3400	34, 34				16

separately performs sparse learning (Dettmers & Zettlemoyer, 2019) to train a sparse ResNet18 model and meet a fixed parameter density d, starting from a random sparse mask. At the end of each round, clients send their updates to the server, where they get aggregated using FedAvg. We name this *naive sparse training (NST)* due to its plug-and-play nature of deployment of sparse learning in FL. Notably, NST can decrease only communication from clients to the server mainly because these updates usually have different sparsity patterns. Therefore, aggregating them by simply averaging of gradients causes the final model to have density $>> d$, translating to a higher downlink communication cost.

Observation 1. *At ultra-low density $d \leq 0.1$, the collaboratively learned FL model significantly sacrifices performance, while the centralized sparse learning yields close to baseline performance.*

As shown in Fig.2, naive deployment of sparse learning in FL causes a noticeable accuracy drop compared to the dense training. In particular, for $d = 0.1$, the model suffers an accuracy drop of 3.67%. This drop becomes more significant for density $d = 0.05$ and increases to 12.03%, hinting at serious limitations of sparse learning in FL. However, the same sparse learning method can yield performance close to the baseline accuracy at $d = 0.05$ in centralized learning.

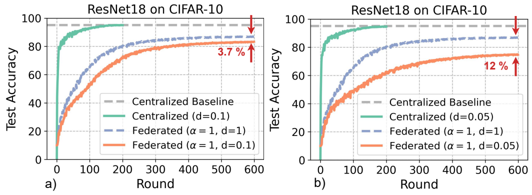

Figure 2: Accuracy vs. round. Dense and Sparse models are shown in dashed and solid lines.

Observation 2. *As the training progresses, the sparse masks in centralized training tend to agree across epochs, showing its convergence, while the server mask in FL does lack agreement and hence lacks of consensus across rounds.*

Definition 1. Sparse mask mismatch. For two models at rounds i and j, we can name the masks associated with their weights $\mathcal{M}^i$ and $\mathcal{M}^j$, and define the *sparse mask mismatch* (SM) $\texttt{sm}^{(i,j)}$ as the Jaccard distance as follows where $\mathcal{M}^i_l$ represents the sparse mask tensor for layer l.

$$\texttt{sm}^{(i,j)} = 1 - \frac{(\sum_{l=1}^{L} \mathcal{M}^i_l \cap \mathcal{M}^j_l)}{(\sum_{l=1}^{L} \mathcal{M}^i_l \cup \mathcal{M}^j_l)} \tag{1}$$

Interestingly, as depicted in Fig. 3(a), the SM for centralized learning tends to zero as the training progresses. In contrast, with the same model, dataset and d values, in FL, the SM remains > 0.4 indicating a substantial distinction in the sparse mask learning between centralized and federated learning (Fig. 3(b)).

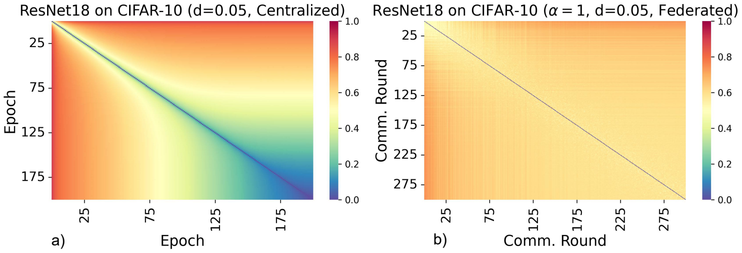

Figure 3: SM for masks generated while sparse learning in (a) centralized and (b) federated learning.

Observation 3. *In federated sparse learning with low target density, the lack of consensus at the later (deeper) layer's masks remains more severe than that of the earlier ones.*

All layers do not carry the same importance towards the final model performance. Similar to earlier works (Ding et al., 2019), we use a popular metric, namely layer pruning sensitivity, to identify layer importance.

Definition 2. Layer pruning sensitivity. Layer sensitivity of a sparse layer is measured via the proxy of the ratio of the total # of non-zero weights to the total # of weights of that layer.

$$\texttt{sensitivity} = \frac{\texttt{\# of non-zero weights in a layer}}{\texttt{\# of total weights of the layer}} \tag{2}$$

As the training progresses, in centralized learning, each layer's mask shows a convergence trend as measured by SM for the layer (Fig. 4(a)). However, Fig. 4(b) shows in FL, the later layers' masks differ significantly and continue to disagree over rounds with SM value as high as ∼0.8. One possible explanation for this phenomenon is the number of parameters per layer and layer sensitivity. In other words, later layers usually have lower sensitivity and a larger number of total parameters allowing these layers to have many possible mask options compared to the earlier layers. Therefore, clients are unlikely to reach a consensus and are more likely to come up with different masks in the later layers, causing an increased SM. For example, 90% of the parameters in layer 1 and 5% layer 14 are present in the final mask, and as expected, SM for these layers is 0 and ∼0.73, respectively.

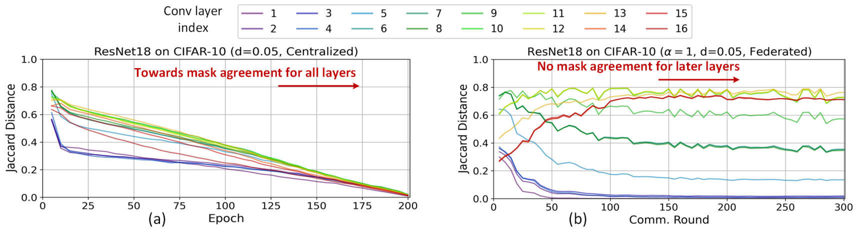

Figure 4: Layer-wise sparse mask mismatch vs. epoch (rounds) for (a) centralized and (b) FL. In FL, the SM for later layers stays high, contrary to centralized, where SM reduces for all layers as the training matures.

To further investigate the impact of higher SM and layer sensitivity on a model's accuracy, we performed five different training in centralized as described in Table 2. Particularly, for the training in row 1 we randomly generate sparse masks with uniform density for all the layers. For all other rows, first, we randomly create each layer's mask by following its pruning sensitivity[2], then decide to keep the layer mask frozen for some or all the layers. More specifically, for rows $3-5$, we allow a fraction of the mask in the mentioned layer to differ between consecutive epochs to meet the target SM value, creating non-convergent masks. As Table 2 clearly shows that large SM (meaning less consensus) for the layers can degrade the accuracy by up to 9.34%, we can safely conclude that *disagreement of masks across epochs can significantly affect the final performance.* Moreover, the model trained via sparse learning with sensitivity-driven pre-defined masks yields better performance than the one trained using a predefined mask.

Table 2: Performance based on the different levels of mask disagreement in centralized.

Training method	Use sensitivity	Masks change at	Layer SM	Test acc%
Pre-defined w/ mask frozen	N	–	–	89.72
Pre-defined w/ mask frozen	Y	–	–	91.66
w/o mask frozen	Y	layer 9-16	0.8	88.88
	Y	layer 1-16	0.5	84.62
	Y	layer 1-16	0.8	82.32

Based on this observation, we hypothesize that such lack of consensus impacts the performance of the final model primarily due to immature learning of the non-zero weight parameters. Thus faster agreement essentially means better trainability of the active (or non-zero) weights. As changing the mask during every epoch essentially means a large chunk of weights to be updated from 0, it may affect the maturity of the trained weights. We want to note that while this is shown for the centralized setting, we believe this is a generic phenomenon irrespective of the centralized or decentralized nature of training.

---

[2] We use another pre-trained model of the same architecture and target d to evaluate sensitivity.

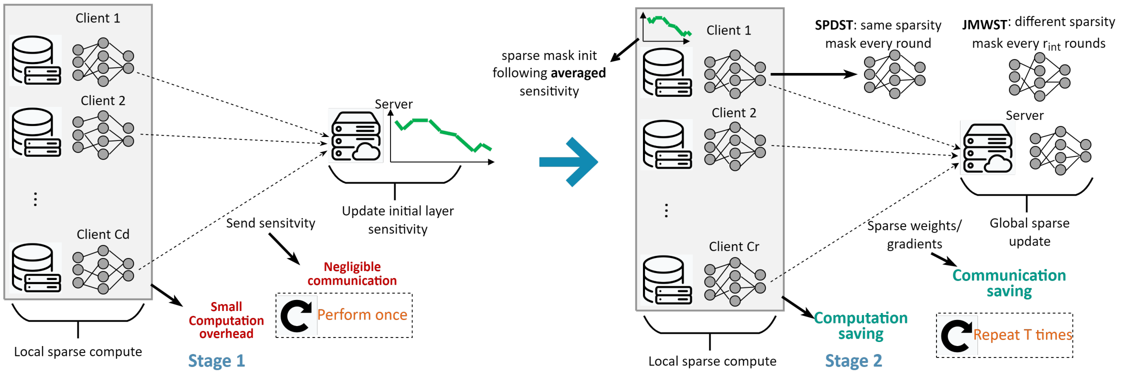

Figure 5: Summary of FLASH. `Stage 1`: C_d clients perform sparse training locally to find layer-wise sensitivities. `Stage 2`: Clients collaboratively train the weights under the server's supervision to follow the layer sensitivities and reach a consensus in yielding sparse masks.

4 FLASH: Methodology

Based on observations in section 3, we hypothesize that deploying sparse learning in clients, though, helps them find a lottery ticket, fails in finding a global one. To help FL find the winning lottery; we identify two key characteristics of sparse learning, *pruning sensitivity* and *mask convergence* and present federated lottery aware sparsity hunting (FLASH) methodologies. To adhere to the identified feature, FLASH includes two stages; `Stage 1` that learns layer sensitivity to properly initialize the sparse mask; `Stage 2` that trains weights and masks. Below, we explain how each step works and highlight its importance. Algorithm 1 details the training methods, and Fig. 5 summarizes FLASH and its components.

4.1 `Stage 1`: Mask Initialization

The goal of this stage is to identify a good sparse mask that the server can provide to the participating clients. However, in FL, the server does not have access to clients' private data. Hence to estimate layer importance, we start by randomly selecting a small fraction of clients ($[\mathcal{C}_d]$) and allow them to perform sparse learning (locally) on their private data for a few warm-up epochs (E_d) (L4-8 in Algo. 1). We then evaluate each of c_d clients' layer sensitivity via Eq. 2. For each layer l, the server estimates average density [3] by averaging the sensitivity of that layer over c_d clients, i.e. $\hat{d}^l = \frac{\sum_{i=1}^{c_d} d_i^l}{c_d}$, where d_i^l is the density at layer l in i^{th} client. As these averaged layer-wise density values may not necessarily satisfy the target density (d) criteria, for a model with K parameters, we present the following *density re-calibration* formulation

$$d_c^l = \hat{d}^l.r_f, \text{ where } r_f = \frac{d \times K}{\sum_{l=1}^{L} \hat{d}^l.k^l} \tag{3}$$

k^l is the dense model's parameter size for layer l. For each layer l of the model, the server then creates a binary sparse mask tensor that is randomly initialized with a fraction of 1s $\propto d_c^l$ (L9-9 in Algo. 1).

4.2 `Stage 2`: Sensitivity-aware Training

Using `Stage 1`, clients can start training with a sensitivity-driven initialized mask. However, this does not guarantee the mask convergence which we have shown (section 3, Obs. 2), is critical. Therefore, we propose the following two approaches that can provide significant improvement in mask convergence.

Approach 1: SPDST. In this approach, to achieve a convergent mask and low `sm` values, the server predefines layer masks at initialization (set $freez = 1$ at $L11$ in Algo. 1). This way, all the clients agree on the mask and only train the non-zero weights. This guarantees no mask divergence issue ($\texttt{sm}^{(i,j)} = 0$ for all i, j).

---

[3] which is the same as sensitivity for a layer.

Algorithm 1: FLASH Training.

```
   Data: Training rounds $T$, local epochs $E$, clients $[\mathcal{C}_N]$, clients per rounds $c_r$, target density $d$ ,
         sensitivity warm-up epochs $E_d$, density warm up client $c_d$, $freez = 0$ and Aggregation type $Agr$.
1  $\mathcal{M}^{init} \leftarrow$ createRandomMask($d$)
2  $\Theta^{init} \leftarrow$ initMaskedWeight($\mathcal{M}^{init}$)
3  serverExecute:
4  Randomly sample $c_d$ clients $[\mathcal{C}_d] \subset [\mathcal{C}_N]$
5  for each client $c \in [\mathcal{C}_d]$ in parallel do
6      $\Theta_c \leftarrow$ clientExecute($\Theta^{init}, E_d, 0$) # $freez = 0$
7      $\mathcal{S}_c \leftarrow$ computeSensitivity($\Theta_c$)
8  end
9  $\mathcal{M}^0 \leftarrow$ initMask($[\mathcal{S}_c], d$)
10 $\Theta^0 \leftarrow$ initMaskedWeight($\mathcal{M}^0$)
11 $freez \leftarrow 1$ if SPDST, 0 if JMWST
12 # Start Stage 2
13 for each round $t \leftarrow 1$ to $T$ do
14     Randomly sample $c_r$ clients $[\mathcal{C}_r] \subset [\mathcal{C}_N]$
15     for each client $c \in [\mathcal{C}_r]$ in parallel do
16         $\Theta_c^t \leftarrow$ clientExecute($\Theta^{t-1}, E, freez$)
17     end
18     $\Theta_S^t \leftarrow$ aggrParamUpdateMask($[\Theta_c^t], Agr$)
19     $\Theta^t \leftarrow$ subsampleServerModel($\Theta_S^t, [\Theta_c^t], d, freez$)
20 end
21 return $\Theta^T$
22 clientExecute($\Theta_c, E, freez$) :
23 $\Theta_{c^0} \leftarrow \Theta_c$
24 for local epoch $i \leftarrow 1$ to $E$ do
25     $\Theta_{c^i} \leftarrow$ doSparseLearning($\Theta_{c^{i-1}}, freez$)
26     $freez \leftarrow$ checkUpdateMask()
27 end
28 return $\Theta_{c^E}$
```

Moreover, as FLASH disentangles the sensitivity evaluation stage from the training, the pre-defined mask in this scenario benefits from the notion of layer sensitivity. We thus aptly name this approach as *sensitivity-driven pre-defined sparse training* (SPDST). Interestingly, earlier research (Bibikar et al., 2022) hinted at poor model performance with pre-defined masks, contrasting ours where we see significantly improved model performance, implying the importance of `stage 1` (as will be elaborated in section 5).

Approach 2: JMWST. Here, after `stage 1`, the global mask is not frozen, and clients have the freedom to come up with their mask and change the global one (set $freez = 0$ at $L11$ in Algo. 1). This way, the model masks, and weights are jointly learned during clients' local learning, thus termed as *joint mask weight sparse training* (JMWST). However, as highlighted earlier, clients' naive sparse mask selection at the beginning of each round costs a considerable accuracy drop (section 3 Obs. 1). To avoid this problem and increase mask consensus, JMWST allows the server to subsample a sparse model with density d at round $t+1$ from the aggregated model at the end of round t.

As mentioned in section 3, with target density d, the aggregated model has density $d_S > d$. To enable efficient sampling of a sparse model while adhering to layer sensitivity, we leverage the density re-calibration strategy (Eq. 3) by taking the t^{th} round's clients' average sensitivity into consideration ($L19$ in Algo. 1). The server performs magnitude pruning to retain the top-d_c^l fraction of parameters for l^{th} layer and sends the pruned model to clients at round $t+1$. Intuitively, the server's sampling of non-zero weights reduces the chances of wasted updates and accelerates mask convergence due to alignment with the layers' pruning sensitivity. Then, the next round's clients can perform sparse learning locally, yield another set of sparse models, send them to the server, and so on. By default, the server evaluates masks every round $r_{int} = 1$. However, it can increase the update interval, and clients update the mask after a specific $r_{int} > 1$ round.

SPDST vs. JMWST. The update aggregation and communication are more straightforward in SPDST, as the position of the zero and non-zero parameters are fixed, and the global model's density remains at d both at the server and the clients. In terms of yielding convergent masks, we indeed observed a lower `sm` for JMWST by $\sim$85% compared to that in NST, evaluated after 300 rounds on CIFAR-10 and `sm` is always 0 for SPDST because the mask is pre-defined. Finally, JMWST gives more freedom to the client, and they can participate in mask training, while in SPDST, the mask is fixed and defined by the server.

Extension to support heterogeneous density. In the current framework, it is assumed that all the clients train with the same target density d. However, users may have different resource limitations, and some may contribute more resources to the training based on their budget. To support this resource-heterogeneity of users and adhere to their respective density budget, we now present hetero-FLASH.

Let us assume there are N available support densities $d_{set} = [d_1, .., d_M]$, where $d_i < d_{i+1}$. Now, for hetero-SPDST and hetero-JMWST, we perform the same `Stage 1` as explained before to create the masks for the clients with the highest density d_N. For any other density d_i, we sample a sparse mask from that with density d_{i+1}. Note, while creating the mask from d_{i+1} to d_i, we follow the layer-wise density re-calibration approach (Eq. 3). Similar to the original SPDST, after `Stage 1`, the server freezes all the N pre-defined mask for the heterogeneous case, and for the rest of the training, clients can use the mask associated with their budget. For hetero-JMWST, at the beginning of each round, the server performs magnitude pruning to yield N sub-models meeting N different density levels, contrasting to the creation of one model in JMWST. Participating clients of different densities use the corresponding sub-models to start sparse learning locally.

In hetero-FLASH, clients do not contribute to weights equally. Considering all the parameters from clients with sparse masks, specifically, the pruned parameters may hurt the updates that are not zero on that same position. Therefore, instead of FedAvg., the server performs aggregation we call *weighted fed averaging* (WFA). In particular, with similar inspiration as Diao et al. (2020), instead of averaging over # of participating clients, we average each non-zero update by their total non-zero occurrences over the participating clients in a round. We have provided the algorithm for hetero-FLASH in the Appendix.

5 Experiments

Datasets and Models. We evaluated the performance of FLASH on MNIST(LeCun & Cortes, 2010) on MNISTNet (McMahan et al., 2017), Federated EMNIST (FEMNIST) (Caldas et al., 2018a) on model described in (Caldas et al., 2018a) and CIFAR-10, CIFAR-100 (Krizhevsky et al., 2009) and TinyImageNet (Pouransari & Ghili, 2014) on ResNet18 (Further details in the Appendix). For data partitioning of MNIST, CIFAR-10, CIFAR-100 and TinyImageNet, we use Latent Dirichlet Allocation (LDA)(Reddi et al., 2020) with three different α ($\alpha = 1000$ for IID and $\alpha = 1$ and 0.1 for non-IID). FEMNIST is built from handwriting 3400 different users (Han et al., 2020); making it inherently non-IID.

Training Hyperparameters. We use starting learning rate (η_{init}) as 0.1 which exponentially decayed to 0.001 (η_{end}). Specifically, learning rate for participants at round t is $\eta_t = \eta_{init}(\mathtt{exp}(\frac{t}{T}\mathtt{log}(\frac{\eta_{init}}{\eta_{end}})))$. In all the sparse learning experiments, the pruning rate is 0.25[4]. Other training hyperparameters can be found in 1. Furthermore, all the results are averaged over three different seeds.

5.1 Experimental Results with FLASH

To understand the importance of `stage 1` in FLASH methodology, we identify a baseline training with uniform layer sensitivity driven *pre-defined sparse training* (PDST) in FL. Table 3 details the performance of FLASH at different levels of d. In particular, as we can see in Table 3 columns 5 and 6, the performance of both NST and PDST produced models cost accuracy drop at ultra low parameter density $d = 0.05$. For example, on CIFAR-10 ($\alpha = 0.1$), models from NST and PDST sacrifice accuracy of 16.35% and 5.32%, respectively. However, at comparatively higher density ($d = 0.1$), both can yield models with a lower accuracy

---

[4] Prune rate controls the fraction of non-zero weights participating in the prune-regrow during sparse learning.

Table 3: Results for different datasets with FLASH (SPDST, and JMWST) and its comparison with NST and PDST for different densities ($d \in \{5\%, 10\%\}$ for all datasets and extreme sparse, $d = 1\%$ for CIFAR-10, CIFAR-100 and TinyImageNet) and data distributions ($\alpha \in \{0.1, 1, 1000\}$).

Dataset	**Data Distribution**	**Density (d)**	**Baseline Acc %**	**NST Acc %**	**PDST Acc %**	**SPDST Acc %**	**JMWST($r_{int} = 1$) Acc %**	**JMWST($r_{int} = 5$) Acc %**
MNIST	IID ($\alpha = 1000$)	1.0	98.79 ± 0.06	–	–	–	–	–
		0.1	–	97.57 ± 0.11	97.09 ± 0.18	$\mathbf{98.21 \pm 0.06}$	97.95 ± 0.16	98.09 ± 0.16
		0.05	–	95.19 ± 0.56	94.8 ± 1.04	$\mathbf{97.46 \pm 0.14}$	97.24 ± 0.21	97.37 ± 0.23
	non-IID ($\alpha = 1.0$)	1.0	98.76 ± 0.06	–	–	–	–	–
		0.1	–	97.36 ± 0.19	96.82 ± 0.25	97.96 ± 0.13	97.72 ± 0.12	$\mathbf{98.11 \pm 0.12}$
		0.05	–	95.75 ± 0.31	95.34 ± 0.77	97.3 ± 0.26	97.38 ± 0.11	$\mathbf{97.59 \pm 0.07}$
	non-IID ($\alpha = 0.1$)	1.0	98.45 ± 0.17	–	–	–	–	–
		0.1	–	96.19 ± 0.22	94.41 ± 1.23	$\mathbf{97.22 \pm 0.43}$	96.53 ± 0.19	96.7 ± 0.14
		0.05	–	91.66 ± 1.74	91.06 ± 1.1	95.7 ± 0.37	95.83 ± 0.84	$\mathbf{95.91 \pm 0.64}$
CIFAR-10	IID ($\alpha = 1000$)	1.0	88.56 ± 0.06	–	–	–	–	–
		0.1	–	84.89 ± 0.26	86.72 ± 0.09	$\mathbf{88 \pm 0.28}$	87.62 ± 0.35	87.86 ± 0.13
		0.05	–	77.48 ± 0.54	84.38 ± 0.12	86.99 ± 0.14	86.87 ± 0.08	$\mathbf{87.18 \pm 0.09}$
		0.01	–	52.70 ± 1.17	70.17 ± 0.70	82.35 ± 0.14	83.59 ± 0.38	$\mathbf{83.85 \pm 0.26}$
	non-IID ($\alpha = 1.0$)	1.0	87.13 ± 0.18	–	–	–	–	–
		0.1	–	83.46 ± 0.19	85.07 ± 0.24	$\mathbf{86.42 \pm 0.49}$	$\mathbf{86.45 \pm 0.31}$	86.36 ± 0.13
		0.05	–	75.1 ± 0.76	83.33 ± 0.14	85.64 ± 0.58	85.34 ± 0.27	$\mathbf{85.9 \pm 0.24}$
		0.01	–	50.71 ± 0.99	69.44 ± 0.63	81.01 ± 0.50	$\mathbf{82.38 \pm 0.18}$	82.31 ± 0.12
	non-IID ($\alpha = 0.1$)	1.0	77.64 ± 0.49	–	–	–	–	–
		0.1	–	71.18 ± 1.23	74.82 ± 0.72	$\mathbf{76.74 \pm 1.46}$	74.74 ± 1.07	75.47 ± 1.18
		0.05	–	61.29 ± 2.76	72.32 ± 1.05	75.47 ± 2.31	73.9 ± 1.45	$\mathbf{75.49 \pm 0.9}$
		0.01	–	42.66 ± 0.50	59.30 ± 0.36	70.61 ± 1.82	68.89 ± 0.62	$\mathbf{71.21 \pm 1.98}$
CIFAR-100	IID ($\alpha = 1000$)	1.0	65.38 ± 0.27	–	–	–	–	–
		0.1	–	53.81 ± 0.92	61.16 ± 0.51	62.35 ± 0.40	$\mathbf{62.88 \pm 0.26}$	62.69 ± 0.24
		0.05	–	42.08 ± 0.48	56.67 ± 0.25	60.32 ± 0.27	59.59 ± 0.19	$\mathbf{60.29 \pm 0.16}$
		0.01	–	22.64 ± 0.75	38.99 ± 1.16	49.67 ± 0.49	51.53 ± 0.76	$\mathbf{51.81 \pm 0.13}$
	non-IID ($\alpha = 1.0$)	1.0	65.17 ± 0.27	–	–	–	–	–
		0.1	–	53.36 ± 0.51	60.87 ± 0.40	$\mathbf{62.13 \pm 0.26}$	61.59 ± 0.07	61.66 ± 0.11
		0.05	–	42.48 ± 0.39	56.57 ± 0.28	59.57 ± 0.35	59.27 ± 0.62	$\mathbf{59.85 \pm 0.35}$
		0.01	–	23.39 ± 0.37	38.99 ± 0.34	49.05 ± 0.40	50.60 ± 0.10	$\mathbf{51.61 \pm 0.66}$
	non-IID ($\alpha = 0.1$)	1.0	59.12 ± 0.63	–	–	–	–	–
		0.1	–	49.04 ± 0.57	55.06 ± 0.26	$\mathbf{56.79 \pm 0.33}$	54.74 ± 0.68	55.54 ± 0.71
		0.05	–	37.33 ± 0.39	51.68 ± 0.32	$\mathbf{54.34 \pm 0.17}$	52.67 ± 0.97	53.47 ± 0.49
		0.01	–	19.21 ± 0.19	35.59 ± 0.26	45.10 ± 0.64	45.31 ± 0.57	$\mathbf{46.16 \pm 0.76}$
TinyImageNet	IID ($\alpha = 1000$)	1.0	55.36 ± 0.25	–	–	–	–	–
		0.1	–	44.63 ± 0.17	51.95 ± 0.11	$\mathbf{53.18 \pm 0.41}$	52.05 ± 0.09	52.51 ± 0.35
		0.05	–	38.39 ± 0.14	48.61 ± 0.25	$\mathbf{51.31 \pm 0.41}$	50.37 ± 0.48	50.53 ± 0.54
		0.01	–	20.50 ± 0.43	37.85 ± 0.07	43.66 ± 0.35	43.07 ± 0.80	$\mathbf{44.41 \pm 0.17}$
	non-IID ($\alpha = 1.0$)	1.0	54.76 ± 0.35	–	–	–	–	–
		0.1	–	44.48 ± 0.16	50.50 ± 0.06	$\mathbf{52.75 \pm 0.18}$	51.22 ± 0.30	51.81 ± 0.08
		0.05	–	38.03 ± 0.27	47.52 ± 0.29	$\mathbf{51.07 \pm 0.23}$	49.48 ± 0.23	49.76 ± 0.48
		0.01	–	20.88 ± 0.14	37.49 ± 0.52	42.91 ± 0.24	43.04 ± 0.12	$\mathbf{43.15 \pm 0.25}$
	non-IID ($\alpha = 0.1$)	1.0	48.12 ± 0.16	–	–	–	–	–
		0.1	–	38.92 ± 0.23	42.64 ± 0.40	$\mathbf{46.25 \pm 0.07}$	45.18 ± 0.38	45.21 ± 0.18
		0.05	–	32.81 ± 0.66	40.69 ± 0.43	$\mathbf{44.56 \pm 0.10}$	43.31 ± 0.19	44.29 ± 0.16
		0.01	–	18.01 ± 0.13	33.79 ± 0.15	37.80 ± 0.06	37.32 ± 0.51	$\mathbf{38.32 \pm 0.19}$
FEMNIST	non-IID	1.0	84.68 ± 0.20	–	–	–	–	–
		0.1	–	76.92 ± 0.42	76.01 ± 1.26	82.70 ± 0.26	83.02 ± 0.21	$\mathbf{83.4 \pm 0.26}$
		0.05	–	37.33 ± 0.39	51.68 ± 0.32	$\mathbf{54.34 \pm 0.17}$	52.67 ± 0.97	53.47 ± 0.49

difference from the baseline by around 6.46% and 2.82%. SPDST, on the other hand, can maintain **close to the baseline accuracy** at even ultra-low density for all data partitions and, interestingly, even outperform JMWST for the majority of the cases. *These results clearly highlight the efficacy of both sensitivity-driven sparse learning (as SPDST > PDST) and early mask convergence (as SPDST ≈ JMWST) in FL settings. Importantly, for increased r_{int} in JMWST, we observe a consistent improvement in accuracy.* The inferior accuracy at $r_{int} = 1$ can be attributed to the mask divergence caused by frequent noisy gradient updates. We thus believe efficient hyperparameter search including r_{int} is essential for the sparse FL model's improved performance, particularly for JMWST. Moreover, JMWST requires additional communication of non-zero weight indices for rounds that masks are updating, contrasting SPDST, where clients do not need to send the mask at all, *allowing us to yield proportional communication saving as the model density.* Fig. 6 shows the accuracy vs. communication round for the two proposed methods on different data distributions.

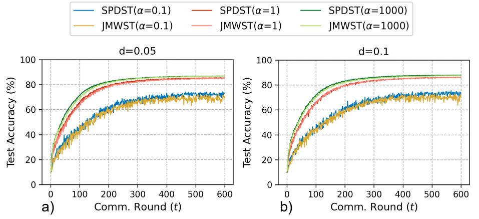

Figure 6: Test accuracy vs. round for CIFAR-10 with (a) $d = 0.05$ (b) $d = 0.1$.

Comparison with ZeroFL. Despite leveraging a form of sparse learning (Raihan & Aamodt, 2020), ZeroFL required significantly higher up-link/down-link communication cost compared to the target density d to achieve better performance. However, FLASH reaches considerably better accuracy while being substantially more efficient in communication compared to ZeroFL. Especially for SPDST, as the mask is frozen throughout the training, the server and clients are only required to communicate updates with density d and enjoy bidirectional savings. Note that every sparse matrix representation requires the value and location of non-zero parameters, but SPDST can get rid of sending the location information because the mask does not change. Finally, we evaluate the communication saving as the ratio of the dense model size and corresponding sparse model size with the tensors represented in a compressed sparse row (CSR) format (Tinney & Walker, 1967). As depicted in Table 4[5], FLASH can yield an accuracy improvement of up to 10.1% at a reduced communication cost of up to 10.26× (computed at up-link when both send sparse models).

Table 4: Comparison with ZeroFL on various performance metrics. (ZeroFL values are the results with the higher accuracy and taken from the original manuscript.)

Dataset	Data Distribution	Method	Density	Acc%	Down-link Savings	Up-link Savings
CIFAR-10	IID	ZeroFL (Qiu et al., 2021)	0.1	*82.71 ± 0.37*	1×	1.6×
		SPDST (ours)	0.1	**88 ± 0.28**	**9.8**×	**9.8**×
		ZeroFL (Qiu et al., 2021)	0.05	*78.22 ± 0.35*	1×	1.9×
		SPDST (ours)	0.05	**86.99 ± 0.14**	**19.5**×	**19.5**×
	non-IID ($\alpha = 1.0$)	ZeroFL (Qiu et al., 2021)	0.1	*81.04 ± 0.28*	1×	1.6×
		SPDST (ours)	0.1	**86.42 ± 0.49**	**9.8**×	**9.8**×
		ZeroFL (Qiu et al., 2021)	0.05	*75.54 ± 1.15*	1×	1.9×
		SPDST (ours)	0.05	**85.64 ± 0.58**	**19.5**×	**19.5**×
FEMNIST	non-IID	ZeroFL (Qiu et al., 2021)	0.05	*77.16 ± 2.07*	1×	**17.7**×
		SPDST (ours)	0.05	**81.18 ± 0.36**	**14.6**×	14.6×

Extreme Sparse Learning. For CIFAR-10 and CIFAR-100, which are trained on a comparably more complex model (ResNet18), we also explore the extremely sparse training scenario where clients train only 1% of the weights, which can translate to up to 100× saving in communication. This experiment particularly shows the importance of both stages in FLASH in achieving a good performance while the performance gap between the dense model and NST or PDST remarkably increases.

5.2 Experimental Results with Hetero-FLASH

Table 5 shows the performance of hetero-FLASH for the scenario where the clients can have three possible density budgets defined by the d_{set} with maximum clients' density $d_{max} = 0.2$. Also, we assume 40%, 30%, and 30% of total clients can train models with a density equal to 0.2, 0.15, and 0.1, respectively. For every round, the server samples 10% from each set with the corresponding target density. Similar to the trend in FLASH, hetero-SPDST outperforms the JMWST counterparts by up to 3.93% evaluated on the three datasets. Also, following a similar trend as with homogeneous density clients, with increased mask update interval (r_{int}), the performance of hetero-JMWST gets a significant boost in accuracy of up to 3.04%.

5.3 Quantitative Analysis on FLASH's Design Parameters

Impact of initial sensitivity warm-up of participating clients. For a realistic scenario, `Stage 1` needs to be efficient and possible. To be more precise, we cannot expect participating clients to train their models

---

[5] We understand for FEMNIST, ZeroFL reported significantly higher up-link saving, however, to the best of our understanding, it should be similar to their report on other datasets, i.e. ∼1.9×.

Table 5: Performance of hetero-FLASH on various datasets where each client can have a density from the set $d_{set} \in [0.1, 0.15, 0.2]$ based on their budget, Note that the density of the final model depends on d_{max}.

Dataset	Data Distribution	Max d_{set}	Hetero-SPDST Acc %	Hetero-JMWST ($r_{int} = 1$) Acc %	Hetero-JMWST ($r_{int} = 5$) Acc %
MNIST	IID ($\alpha = 1000$)	0.2	$\mathbf{98.29 \pm 0.05}$	97.44 ± 0.23	97.83 ± 0.10
	non-IID ($\alpha = 1.0$)		$\mathbf{98.29 \pm 0.09}$	97.47 ± 0.22	97.80 ± 0.23
	non-IID ($\alpha = 0.1$)		$\mathbf{97.63 \pm 0.22}$	96.11 ± 0.75	96.25 ± 0.86
CIFAR-10	IID ($\alpha = 1000$)	0.2	87.19 ± 0.26	86.37 ± 0.2	$\mathbf{87.39 \pm 0.15}$
	non-IID ($\alpha = 1.0$)		86.16 ± 0.04	84.67 ± 0.06	$\mathbf{86.19 \pm 0.24}$
	non-IID ($\alpha = 0.1$)		$\mathbf{75.23 \pm 1.26}$	71.3 ± 2.75	74.34 ± 0.85
CIFAR-100	IID ($\alpha = 1000$)	0.2	63.4 ± 0.2	60.5 ± 0.8	$\mathbf{62.91 \pm 0.04}$
	non-IID ($\alpha = 1.0$)		62.1 ± 0.2	59.6 ± 0.2	$\mathbf{62.68 \pm 0.28}$
	non-IID ($\alpha = 0.1$)		56.4 ± 0.4	51.5 ± 0.9	$\mathbf{55.98 \pm 0.19}$
TinyImageNet	IID ($\alpha = 1000$)	0.2	51.28 ± 0.11	49.73 ± 0.20	$\mathbf{52.07 \pm 0.22}$
	non-IID ($\alpha = 1$)		50.94 ± 0.17	49.32 ± 0.16	$\mathbf{51.61 \pm 0.17}$
	non-IID ($\alpha = 0.1$)		44.48 ± 0.40	42.72 ± 0.61	$\mathbf{44.65 \pm 0.45}$
FEMNIST	non-IID	0.2	$\mathbf{82.58 \pm 0.24}$	82.2 ± 0.42	82.5 ± 0.55

for a long time in order to get an accurate estimation of layer sensitivity. Also, it is unlikely to access many clients in a single time slot, especially in cross-device federated learning. Therefore, we designed six different scenarios to understand the impact of these parameters on the final model's performance. In particular, we used two different values of participating clients ([10, 20]) and three local epoch choices ([10, 20, 40]). As shown in Fig. 7(a), the yielded pruning sensitivity follows a similar trend. Moreover, SPDST with a mask chosen from any of these sensitivity lists finally yields FL models with similar performances (Fig. 7(b)), clearly demonstrating the robustness of our warm-up based sensitivity evaluation `stage 1`.

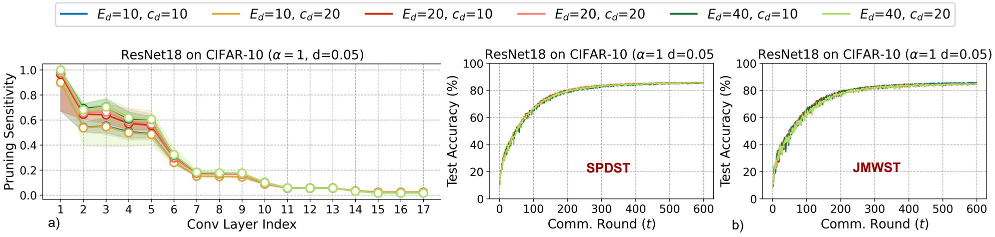

Figure 7: (a) Layer sensitivity evaluated at the end of sensitivity warm-up stage (`Stage 1`) for different client participation (c_d) and their local epochs (E_d), (b) Comparison of global model performance with the initialized sparse mask based on different sensitivity evaluated from (a).

Convergence versus communication costs. Fig. 8(a) and (b) show the performance of FL models when the clients are communication limited. In particular, PDST and SPDST can significantly outperform other approaches at low communication budgets (even FedAvg). This can be attributed to their substantially smaller model sizes, helping them run for higher rounds than others on a limited bandwidth scenario.

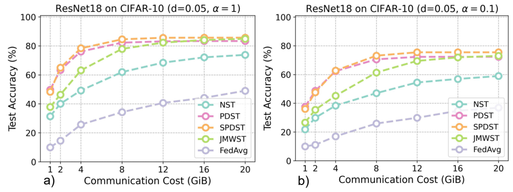

Figure 8: Performance vs. up-link bandwidth for (a) $\alpha = 1.0$ and (b) $\alpha = 0.1$.

Overheads of `stage 1`. `Stage 1` uses one round with E_d local epochs (for us $E_d = 10$) per client. A normal FL stage in our settings trains the clients for T rounds, 1 epoch per client/round. Therefore, this stage increases the time by a factor of $(\frac{E_d}{T} + 1)$. Usually, $E_d << T$, making the pre-training time overhead negligible.

The communication overhead of `Stage 1` is also negligible compared to that in each round for the `Stage 2` FL training. Each participant only needs to send L values for an L-layer model. So, c_d clients will have a total communication overhead of $(L \times c_d \times 32)$ bits, assuming 32-bit number representation.

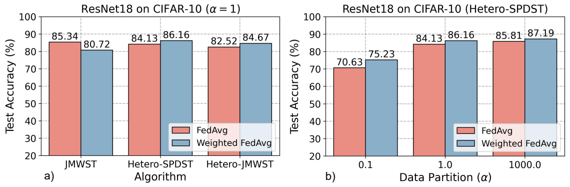

Figure 9: Performance comparison between FedAvg and weighted FedAvg for different (a) algorithms (b) data distributions (α).

Importance weighted aggregation in hetero-FLASH. Earlier literature (Diao et al., 2020) suggested weighted averaging in the aggregation of models with different sizes, which we also investigate here. In particular, we performed experiments on CIFAR-10 ($\alpha = 1.0$), both with and without WFA. First, we observe that WFA degrades model performance in JMWST compared to FedAvg (Fig. 9 (a)). On the contrary, the use of WFA improves accuracy for hetero-FLASH (Fig. 9 (b)). The inferior performance of WFA in FLASH may hint at the fact that if a parameter is non-zero only for fewer clients, as compared to other non-zero weights, giving it equal weight as the others in the aggregation nullifies its lower importance, that may be necessary to preserve for mask convergence. On the other hand, having WFA in hetero FLASH is necessary, as the less frequent non-zero occurrence of a parameter can be a result of the presence of fewer high-parameter density clients in a round.

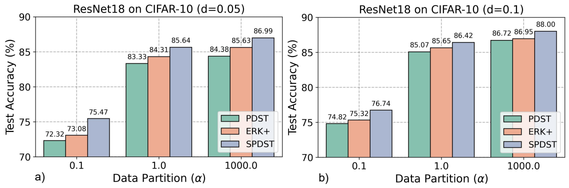

Figure 10: Performance of models trained with SPDST, uniform (PDST) and ERK+ initialized layer-wise parameter density for (a) $d = 0.05$ (b) $d = 0.1$

Comparison with ERK+ initialization. We now compare our SPDST mask initialization with that of parameter density distribution evaluated via ERK+ (Huang et al., 2022; Evci et al., 2020). In contrast with uniform density, the ERK+ scheme keeps more weights for the layers with fewer parameters. To this aim, we use `Stage 1` in SPDST, ERK+, or uniform (PDST) as the initial mask for `stage 2` and keep the mask frozen for the rest of the training. As shown in Fig. 10, the mask initialization using `stage 1` for SPDST consistently provides superior results over the other two. We hypothesize this is rooted in the data-driven layer sensitivity evaluation scheme of SPDST, particularly at the earlier layers, allowing it to retain more information at these layers.

Ablation on `Stage 1`. Our proposed method consists of two stages, sensitivity evaluation (`Stage 1`) and training in federated settings (`Stage 2`). In Table 6, we present ablation with and without `Stage 1` for SPDST and JMWST. It is notable that SPDST without `Stage 1` is PDST.

Table 6: Impact of `Stage 1` on final performance on CIFAR-10 dataset with target $d = 0.05$

Data Distribution	Method	without `Stage 1`	with `Stage 1`
IID($\alpha = 1000$)	SPDST	84.38 ± 0.12	$\mathbf{86.99 \pm 0.14}$
non-IID($\alpha = 0.1$)	SPDST	72.32 ± 1.05	$\mathbf{75.47 \pm 2.31}$
IID($\alpha = 1000$)	JMWST	86.93 ± 0.1	$\mathbf{87.18 \pm 0.09}$
non-IID($\alpha = 0.1$)	JMWST	74.7 ± 1.7	$\mathbf{75.49 \pm 0.9}$

6 Conclusions

This paper presented different methodologies to yield sparse server models with insignificant accuracy drops compared to the unpruned counterparts. In particular, we demonstrated two efficient sparse learning solutions specifically tailored for FL, enabling better computation and communication benefits over existing sparse learning alternatives. We experimentally demonstrated the superiority of our models in yielding up to ~10.1% improved accuracy with ~10.26× less communication costs, compared to SOTA Qiu et al. (2021), at similar hyperparameter settings. Moreover, we also presented the effectiveness of the proposed algorithms with extremely low densities with high communication reduction which can be deployed for highly resource-limited edge devices. The future research direction of this work includes the theoretical understanding of our observations and further empirical demonstrations of newer classes of models including transformers.

References

Sameer Bibikar, Haris Vikalo, Zhangyang Wang, and Xiaohan Chen. Federated dynamic sparse training: Computing less, communicating less, yet learning better. In *Proceedings of the AAAI Conference on Artificial Intelligence*, volume 36, pp. 6080–6088, 2022.

Sebastian Caldas, Sai Meher Karthik Duddu, Peter Wu, Tian Li, Jakub Konečnỳ, H Brendan McMahan, Virginia Smith, and Ameet Talwalkar. Leaf: A benchmark for federated settings. *arXiv preprint arXiv:1812.01097*, 2018a.

Sebastian Caldas, Jakub Konečny, H Brendan McMahan, and Ameet Talwalkar. Expanding the reach of federated learning by reducing client resource requirements. *arXiv preprint arXiv:1812.07210*, 2018b.

Tim Dettmers and Luke Zettlemoyer. Sparse networks from scratch: Faster training without losing performance. *arXiv preprint arXiv:1907.04840*, 2019.

Enmao Diao, Jie Ding, and Vahid Tarokh. Heterofl: Computation and communication efficient federated learning for heterogeneous clients. *arXiv preprint arXiv:2010.01264*, 2020.

Xiaohan Ding, Xiangxin Zhou, Yuchen Guo, Jungong Han, Ji Liu, et al. Global sparse momentum sgd for pruning very deep neural networks. *Advances in Neural Information Processing Systems*, 32, 2019.

Utku Evci, Trevor Gale, Jacob Menick, Pablo Samuel Castro, and Erich Elsen. Rigging the lottery: Making all tickets winners. In *International Conference on Machine Learning*, pp. 2943–2952. PMLR, 2020.

Jonathan Frankle and Michael Carbin. The lottery ticket hypothesis: Finding sparse, trainable neural networks. *arXiv preprint arXiv:1803.03635*, 2018.

Eduard Gorbunov, Konstantin P Burlachenko, Zhize Li, and Peter Richtárik. Marina: Faster non-convex distributed learning with compression. In *International Conference on Machine Learning*, pp. 3788–3798. PMLR, 2021.

Pengchao Han, Shiqiang Wang, and Kin K Leung. Adaptive gradient sparsification for efficient federated learning: An online learning approach. In *2020 IEEE 40th International Conference on Distributed Computing Systems (ICDCS)*, pp. 300–310. IEEE, 2020.

Chaoyang He, Murali Annavaram, and Salman Avestimehr. Group knowledge transfer: Federated learning of large cnns at the edge. *Advances in Neural Information Processing Systems*, 33:14068–14080, 2020.

Kaiming He, Xiangyu Zhang, Shaoqing Ren, and Jian Sun. Deep residual learning for image recognition. In *Proceedings of the IEEE conference on computer vision and pattern recognition*, pp. 770–778, 2016.

Samuel Horvath, Stefanos Laskaridis, Mario Almeida, Ilias Leontiadis, Stylianos Venieris, and Nicholas Lane. Fjord: Fair and accurate federated learning under heterogeneous targets with ordered dropout. *Advances in Neural Information Processing Systems*, 34, 2021.

Tiansheng Huang, Shiwei Liu, Li Shen, Fengxiang He, Weiwei Lin, and Dacheng Tao. Achieving personalized federated learning with sparse local models. *arXiv preprint arXiv:2201.11380*, 2022.

Berivan Isik, Francesco Pase, Deniz Gunduz, Tsachy Weissman, and Michele Zorzi. Sparse random networks for communication-efficient federated learning. *ICLR*, 2023.

Yuang Jiang, Shiqiang Wang, Victor Valls, Bong Jun Ko, Wei-Han Lee, Kin K Leung, and Leandros Tassiulas. Model pruning enables efficient federated learning on edge devices. *IEEE Transactions on Neural Networks and Learning Systems*, 2022.

Peter Kairouz, H. Brendan McMahan, Brendan Avent, Aurélien Bellet, Mehdi Bennis, Arjun Nitin Bhagoji, Kallista Bonawitz, Zachary Charles, Graham Cormode, Rachel Cummings, Rafael G. L. D'Oliveira, Hubert Eichner, Salim El Rouayheb, David Evans, Josh Gardner, Zachary Garrett, Adrià Gascón, Badih Ghazi, Phillip B. Gibbons, Marco Gruteser, Zaid Harchaoui, Chaoyang He, Lie He, Zhouyuan Huo, Ben Hutchinson, Justin Hsu, Martin Jaggi, Tara Javidi, Gauri Joshi, Mikhail Khodak, Jakub Konecný, Aleksandra Korolova, Farinaz Koushanfar, Sanmi Koyejo, Tancrède Lepoint, Yang Liu, Prateek Mittal, Mehryar Mohri, Richard Nock, Ayfer Özgür, Rasmus Pagh, Hang Qi, Daniel Ramage, Ramesh Raskar, Mariana Raykova, Dawn Song, Weikang Song, Sebastian U. Stich, Ziteng Sun, Ananda Theertha Suresh, Florian Tramèr, Praneeth Vepakomma, Jianyu Wang, Li Xiong, Zheng Xu, Qiang Yang, Felix X. Yu, Han Yu, and Sen Zhao. Advances and open problems in federated learning. *Foundations and Trends® in Machine Learning*, 14(1–2):1–210, 2021. ISSN 1935-8237. doi: 10.1561/2200000083. URL `http://dx.doi.org/10.1561/2200000083`.

Alex Krizhevsky, Geoffrey Hinton, et al. Learning multiple layers of features from tiny images. 2009.

Souvik Kundu and Sairam Sundaresan. Attentionlite: Towards efficient self-attention models for vision. In *ICASSP 2021-2021 IEEE International Conference on Acoustics, Speech and Signal Processing (ICASSP)*, pp. 2225–2229. IEEE, 2021.

Souvik Kundu, Saurav Prakash, Haleh Akrami, Peter A Beerel, and Keith M Chugg. psconv: A pre-defined sparse kernel based convolution for deep cnns. In *2019 57th Annual Allerton Conference on Communication, Control, and Computing (Allerton)*, pp. 100–107. IEEE, 2019.

Souvik Kundu, Mahdi Nazemi, Massoud Pedram, Keith M Chugg, and Peter A Beerel. Pre-defined sparsity for low-complexity convolutional neural networks. *IEEE Transactions on Computers*, 69(7):1045–1058, 2020.

Souvik Kundu, Gourav Datta, Massoud Pedram, and Peter A Beerel. Spike-thrift: Towards energy-efficient deep spiking neural networks by limiting spiking activity via attention-guided compression. In *Proceedings of the IEEE/CVF Winter Conference on Applications of Computer Vision*, pp. 3953–3962, 2021a.

Souvik Kundu, Mahdi Nazemi, Peter A Beerel, and Massoud Pedram. Dnr: A tunable robust pruning framework through dynamic network rewiring of dnns. In *Proceedings of the 26th Asia and South Pacific Design Automation Conference*, pp. 344–350, 2021b.

Souvik Kundu, Yao Fu, Bill Ye, Peter A Beerel, and Massoud Pedram. Toward adversary-aware non-iterative model pruning through d ynamic n etwork r ewiring of dnns. *ACM Transactions on Embedded Computing Systems*, 21(5):1–24, 2022.

Yann LeCun and Corinna Cortes. MNIST handwritten digit database. 2010. URL `http://yann.lecun.com/exdb/mnist/`.

Ang Li, Jingwei Sun, Binghui Wang, Lin Duan, Sicheng Li, Yiran Chen, and Hai Li. Lotteryfl: Personalized and communication-efficient federated learning with lottery ticket hypothesis on non-iid datasets. *arXiv preprint arXiv:2008.03371*, 2020a.

Ang Li, Jingwei Sun, Xiao Zeng, Mi Zhang, Hai Li, and Yiran Chen. Fedmask: Joint computation and communication-efficient personalized federated learning via heterogeneous masking. In *Proceedings of the 19th ACM Conference on Embedded Networked Sensor Systems*, pp. 42–55, 2021.

Tian Li, Anit Kumar Sahu, Manzil Zaheer, Maziar Sanjabi, Ameet Talwalkar, and Virginia Smith. Federated optimization in heterogeneous networks. *Proceedings of Machine Learning and Systems*, 2:429–450, 2020b.

Xiang Li, Kaixuan Huang, Wenhao Yang, Shusen Wang, and Zhihua Zhang. On the convergence of fedavg on non-iid data. *arXiv preprint arXiv:1907.02189*, 2019.

Tao Lin, Lingjing Kong, Sebastian U Stich, and Martin Jaggi. Ensemble distillation for robust model fusion in federated learning. *Advances in Neural Information Processing Systems*, 33:2351–2363, 2020.

Shiwei Liu, Decebal Constantin Mocanu, Amarsagar Reddy Ramapuram Matavalam, Yulong Pei, and Mykola Pechenizkiy. Sparse evolutionary deep learning with over one million artificial neurons on commodity hardware. *Neural Computing and Applications*, 33(7):2589–2604, 2021.

Zhuang Liu, Mingjie Sun, Tinghui Zhou, Gao Huang, and Trevor Darrell. Rethinking the value of network pruning. *arXiv preprint arXiv:1810.05270*, 2018.

Brendan McMahan, Eider Moore, Daniel Ramage, Seth Hampson, and Blaise Aguera y Arcas. Communication-efficient learning of deep networks from decentralized data. In *Artificial intelligence and statistics*, pp. 1273–1282. PMLR, 2017.

Yiqun Mei, Pengfei Guo, Mo Zhou, and Vishal Patel. Resource-adaptive federated learning with all-in-one neural composition. *Advances in Neural Information Processing Systems*, 35:4270–4284, 2022.

Decebal Constantin Mocanu, Elena Mocanu, Peter Stone, Phuong H Nguyen, Madeleine Gibescu, and Antonio Liotta. Scalable training of artificial neural networks with adaptive sparse connectivity inspired by network science. *Nature communications*, 9(1):1–12, 2018.

Hadi Pouransari and Saman Ghili. Tiny imagenet visual recognition challenge. *CS231N course, Stanford Univ., Stanford, CA, USA*, 5, 2014.

Eric Qin, Ananda Samajdar, Hyoukjun Kwon, Vineet Nadella, Sudarshan Srinivasan, Dipankar Das, Bharat Kaul, and Tushar Krishna. Sigma: A sparse and irregular gemm accelerator with flexible interconnects for dnn training. In *2020 IEEE International Symposium on High Performance Computer Architecture (HPCA)*, pp. 58–70. IEEE, 2020.

Xinchi Qiu, Javier Fernandez-Marques, Pedro PB Gusmao, Yan Gao, Titouan Parcollet, and Nicholas Donald Lane. Zerofl: Efficient on-device training for federated learning with local sparsity. In *International Conference on Learning Representations*, 2021.

Md Aamir Raihan and Tor Aamodt. Sparse weight activation training. *Advances in Neural Information Processing Systems*, 33:15625–15638, 2020.

Vivek Ramanujan, Mitchell Wortsman, Aniruddha Kembhavi, Ali Farhadi, and Mohammad Rastegari. What's hidden in a randomly weighted neural network? In *Proceedings of the IEEE/CVF Conference on Computer Vision and Pattern Recognition*, pp. 11893–11902, 2020.

Sashank Reddi, Zachary Charles, Manzil Zaheer, Zachary Garrett, Keith Rush, Jakub Konečnỳ, Sanjiv Kumar, and H Brendan McMahan. Adaptive federated optimization. *arXiv preprint arXiv:2003.00295*, 2020.

William F Tinney and John W Walker. Direct solutions of sparse network equations by optimally ordered triangular factorization. *Proceedings of the IEEE*, 55(11):1801–1809, 1967.

Jianyu Wang, Qinghua Liu, Hao Liang, Gauri Joshi, and H Vincent Poor. Tackling the objective inconsistency problem in heterogeneous federated optimization. *Advances in neural information processing systems*, 33: 7611–7623, 2020.

Giyoung Yang and Taewhan Kim. Design and algorithm for clock gating and flip-flop co-optimization. In *2018 IEEE/ACM International Conference on Computer-Aided Design (ICCAD)*, pp. 1–6. IEEE, 2018.

Haoran You, Chaojian Li, Pengfei Xu, Yonggan Fu, Yue Wang, Xiaohan Chen, Richard G Baraniuk, Zhangyang Wang, and Yingyan Lin. Drawing early-bird tickets: Towards more efficient training of deep networks. *arXiv preprint arXiv:1909.11957*, 2019.

Yuchen Zhang, John Duchi, Michael I Jordan, and Martin J Wainwright. Information-theoretic lower bounds for distributed statistical estimation with communication constraints. In C.J. Burges, L. Bottou, M. Welling, Z. Ghahramani, and K.Q. Weinberger (eds.), *Advances in Neural Information Processing Systems*, volume 26. Curran Associates, Inc., 2013. URL `https://proceedings.neurips.cc/paper/2013/file/d6ef5f7fa914c19931a55bb262ec879c-Paper.pdf`.

Aojun Zhou, Yukun Ma, Junnan Zhu, Jianbo Liu, Zhijie Zhang, Kun Yuan, Wenxiu Sun, and Hongsheng Li. Learning n: m fine-grained structured sparse neural networks from scratch. *arXiv preprint arXiv:2102.04010*, 2021.

Zhuangdi Zhu, Junyuan Hong, and Jiayu Zhou. Data-free knowledge distillation for heterogeneous federated learning. In *International Conference on Machine Learning*, pp. 12878–12889. PMLR, 2021.

A Appendix

A.1 Hetero-FLASH Algorithm

Algorithm 2 details the training algorithm in hetero-FLASH. Note that and `aggrParamUpdateMask` and `subSampleServerModel` are the two functions that play a key role in supporting heterogeneity in sparsity ratios for different clients. The details of these two functions are elaborated in Algorithm 3 and 4, respectively. We plan to open-source our code upon acceptance of the paper.

Algorithm 2: Hetero-FLASH Training.

```
Data: Training rounds $T$, local epochs $E$, client set $[[\mathcal{C}_{N_1}], ..., [\mathcal{C}_{N_M}]]$, clients per rounds $c_r$, target density set
      $d_{set} = [d_1, ..., d_M]$, sensitivity warm-up epochs $E_d$, density warm up client count $c_d$, initial value of freeze
      masks $freez = 0$, training algorithm $A$ and aggregation type $Agr$.
$\mathcal{M}^{init} \leftarrow$ createRandomMask()
$\Theta^{init} \leftarrow$ initMaskedWeight($\mathcal{M}^{init}$)
serverExecute:
Randomly sample $c_d$ clients $[\mathcal{C}_d] \subset [\mathcal{C}_{N_M}]$
for each client $c \in [\mathcal{C}_d]$ in parallel do
    $\Theta_c \leftarrow$ clientExecute($\Theta^{init}, E_d, 0$)
    $\mathcal{S}_c \leftarrow$ computeSensitivity($\Theta_c$)
end
$\mathcal{M}^0 \leftarrow$ initMask($[\mathcal{S}_c], d_{set}$)
$\Theta^0 \leftarrow$ initMaskedWeight($\mathcal{M}^0$)
$freez \leftarrow$ freezeMask($A$)
for each round $t \leftarrow 1$ to $T$ do
    Randomly sample $c_r$ clients $[\mathcal{C}_r] \subset [\mathcal{C}_N]$
    for each client $c \in [\mathcal{C}_r]$ in parallel do
        $\Theta_c^t \leftarrow$ clientExecute($\Theta^{t-1}, E, freez$)
    end
    $\Theta_S^t \leftarrow$ aggrParamUpdateMask($[\Theta_c^t], Agr$)
    $\Theta^t \leftarrow$ subSampleServerModel($\Theta_S^t, [\Theta_c^t], d_{set}, freez$)
end
clientExecute($\Theta_c, E, freez$) :
$\Theta_{c^0} \leftarrow \Theta_c$
for local epoch $i \leftarrow 1$ to $E$ do
    $\Theta_{c^i} \leftarrow$ doSparseLearning($\Theta_{c^{i-1}}, m_{c^{freez}}$)
    $freez \leftarrow$ checkUpdateMask()
end
return $\Theta_{c^E}$
```

A.2 Model Architectures

Table 7 shows the model architectures used for MNIST and FEMNIST datasets. For CIFAR-10 we used ResNet18 (He et al., 2016) with the first `CONV` layer kernel size as 3 × 3 instead of original 7 × 7.

A.3 Additional Comparisons

We now compare the performance of FLASH with that of yielded via FedSpa (Huang et al., 2022) and FedDST (Bibikar et al., 2022). For FedSpa, we implemented their proposed algorithm in our settings and kept all the hyperparameters the same for an apple-to-apple comparison. We report the best accuracy yielded for FLASH via models trained using SPDST and JMWST. As shown in Table 8, FLASH outperforms FedSpa up to 2.41%. A similar trend is observed when we compare with FedDST, and as Table 9, on the MNIST dataset, FLASH can have an accuracy improvement of up to 1.41%.

Algorithm 3: `aggrParamUpdateMask`

```
Data: Round $t$, aggregation type $Agr$ [fedAvg, weightedFedAvg], clients updates $[\Theta^t] = [\Theta_{c_1}, ..., \Theta_{c_r}]$, client
      data size $[ds_{c_1}, ..., ds_{c_r}]$
if $Agr$ is fedAvg then
    $\Theta_S^t \leftarrow \frac{1}{\Sigma_{c_i=1}^{c_r} ds_{c_i}} \Sigma_{c_i=1}^{c_r} ds_{c_i} \cdot \Theta_{c_i}^t$
else
    //For hetero-FLASH
    $\mathcal{W}^t \leftarrow$ initWeightFactor()
    for each update $\Theta_{c_i} \in [\Theta^t]$ do
        $\mathcal{W}_{c_i}^t \leftarrow ds_{c_i} \times$ retrieveMask($\Theta_{c_i}$)
        $\mathcal{W}^t \leftarrow \mathcal{W}^t + \mathcal{W}_{c_i}^t$
    end
    //safeDivide(a,b): gives zero anywhere the b is queal to zero
    $\Theta_S^t \leftarrow \Sigma_{c_i=1}^{c_r}$[safeDivide($\mathcal{W}_{c_i}^t, \mathcal{W}^t$) $\cdot \Theta_{c_i}^t$]
end
```

Algorithm 4: `subsampleServerModel`

```
Data: Current round id $t$, client set $[\mathcal{C}_r]$, aggregated Weight $\Theta_S^t$ of model with $L$ layers, support density set $d_{set}$
      $= [d_1, ..., d_M]$ where $d_i < d_{i+1}$, model layer-wise parameter count $[k] = [k^1, ..., k^L]$.
if $size(d_{set})$ is 1 then
    //JMWST subsampling in FLASH
    $\mathcal{M} \leftarrow$ initMaskWithZeros()
    $[\hat{d}^1, ..., \hat{d}^L] \leftarrow$ avgLayerWiseDensity($[\mathcal{C}_r]$)
    $r_f \leftarrow \frac{d_1 \times K}{\sum_{l=1}^{L} \hat{d}^l . k^l}$
    for layer $l \leftarrow 1$ to $L$ do
        idx $\leftarrow$ getSortedWeightIndeices($\Theta_S^t, l$)
        $n_z \leftarrow$ int($r_f \times \hat{d}^l \times k^l$) //number of non-zeros
        $\mathcal{M}^l$[idx[: $n_z$]] $\leftarrow 1$
    end
else
    //For hetero-FLASH
    for $d_i \in d_{set}$ do
        $\mathcal{M}_i \leftarrow$ initMaskWithZeros()
    end
    $\mathcal{D}_s^t \leftarrow$ getCurrentDensity($\Theta_S^t$)
    $[\hat{d}^1, ..., \hat{d}^L] \leftarrow$ getLayerWiseDensity($\Theta_S^t$)
    for layer $l \leftarrow 1$ to $L$ do
        idx $\leftarrow$ getSortedWeightIndeices($\Theta_S^t, l$)
        for $d_i \in d_{set}$ do
            $r_{f_i} \leftarrow \frac{d_i}{\mathcal{D}_s^t}$
            $n_z \leftarrow$ int($r_{f_i} \times \hat{d}^l \times k^l$)
            ${\mathcal{M}_i}^l$[idx[: $n_z$]] $\leftarrow 1$
        end
    end
end
```

B More Quantitative Analysis

Below we provide more analysis and ablation to show the effectiveness of FLASH in different scenarios.

Table 7: Architecture used for MNIST and FEMNIST datasets

MNIST	FEMNIST
$\texttt{CONV}5 \times 5(C_o = 10)$	$\texttt{CONV}5 \times 5(C_o = 32)$
`max_pool`	`max_pool`
$\texttt{CONV}5 \times 5(C_o = 20)$	$\texttt{CONV}5 \times 5(C_o = 64)$
`max_pool`	`max_pool`
$\texttt{FC}(5120, 50)$	$\texttt{FC}(3136, 2048)$
$\texttt{FC}(50, 10)$	$\texttt{FC}(2028, 62)$

Table 8: Comparison of FLASH with FedSpa (Huang et al., 2022) on CIFAR-10 with ResNet18.

Data distribution	Method	Density (d)	Best Acc. (%)	δ_{Acc}
$\alpha = 1000$	FedSpa	0.05	85.63	–
	FLASH	0.05	**87.18**	+1.55
$\alpha = 0.1$	FedSpa	0.05	73.08	–
	FLASH	0.05	**75.49**	+2.41

Table 9: Comparison of FLASH with FedDST (Bibikar et al., 2022) on pathologically non-IID MNIST. We used the same hyperparameter settings and models as in (Bibikar et al., 2022) for this comparison.

Method	Density (d)	Communication Cost (GiB)	Best Acc. (%)	δ_{Acc}
FedDST	0.2	1.0	96.10	–
FLASH			**97.51**	+1.41
FedDST	0.2	2.0	97.35	–
FLASH			**97.69**	+0.34

B.1 Impact of Number of participating clients per round.

Fig. 11 (a) shows that JMWST and SPDST follow the same pattern at the baseline model ($d = 1.0$) with FedAvg. In other words, similar to FedAvg, as the c_r increases, the performance enhances. Also, for a specific c_r, JMWST and SPDST perform better than PDST and NST.

B.2 Impact of Batch-Normalization layer statistics.

Fig 11 (b) shows the performance comparison between batch normalization (BN) and static batch normalization (static BN, as suggested in (Diao et al., 2020)). In particular, in our setting, using BN layer statistics consistently outperform the static BN.

B.3 Effect of the mask update interval rounds (r_{int}) in JMWST.

As mentioned in the original manuscript, for JMWST, the server can increase the mask update interval (r_{int}) to save communication energy. We thus performed ablation for this variable from the default value of 1 (similar to (Qiu et al., 2021)) to see its impact on the final accuracy, and Table 10 and Fig. 12 show the results. In particular, as we can see in the table, less frequent update intervals can lead to better performance than the original JMWST and provide additional bidirectional saving in communication as the masks do not change every round. Fig. 12 also indicates that the improvement tends to saturate after specific r_{int}, which hints at the importance of this parameter. This pattern in the performance means that r_{int} may potentially create a trade-off between the learnability of the masks and weights, and we believe understanding this complex trade-off is an interesting future research.

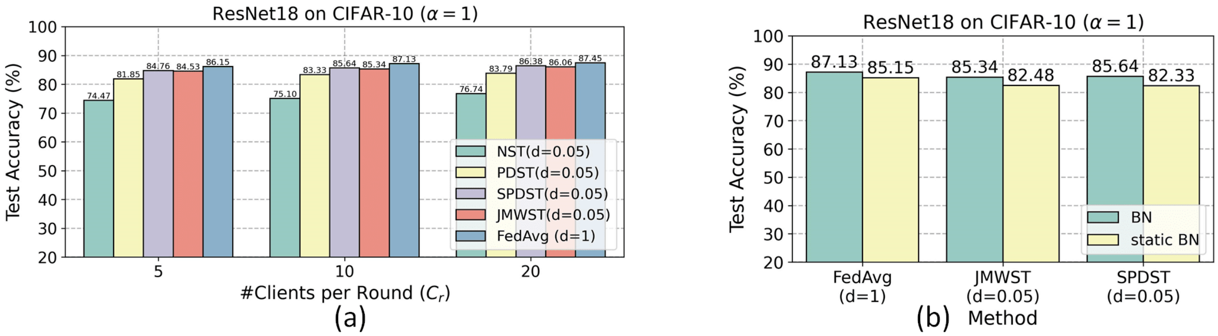

Figure 11: (a) Performance of the final trained model for different participating clients per round, (b) Significance of BN and Static BN in final model performance.

Table 10: Ablation with different mask update intervals for JMWST for a target density $d = 0.1$ on CIFAR-10.

Model	**Data distribution**	**Mask update interval rounds (r_{int})**			
		$r_{int} = 1$	$r_{int} = 2$	$r_{int} = 5$	$r_{int} = 10$
ResNet18	IID ($\alpha = 1000$)	87.62 ± 0.35	87.76 ± 0.07	87.86 ± 0.13	87.67 ± 0.09
	non-IID ($\alpha = 1$)	86.45 ± 0.31	86.26 ± 0.07	86.36 ± 0.13	86.68 ± 0.25
	non-IID ($\alpha = 0.1$)	74.74 ± 1.07	73.73 ± 1.18	75.47 ± 1.08	77.14 ± 0.22

B.4 Convergence trend of proposed algorithms.

Fig. 13 shows the test accuracy vs. FL rounds for NST, PDST, SPDST, and JMWST algorithms on the CIFAR-10 dataset with non-IID data distribution ($\alpha = 1$). As shown in the plots, for $d = 0.05$ and $d = 0.1$, NST has slower convergence with lower final accuracy. Introducing consensus among the clients for the sparse mask accelerates the convergence and enhances the final performance.

B.5 Revisiting sparse mask mismatch for NST with VGG16.

Fig. 14 shows the comparison of SM between centralized and FL settings with NST on VGG16, another popular model variant. Similar to our observed trend with ResNet18, we see a significantly high SM for FL settings with a target of $d = 0.05$. This strengthens the generality of our observed limitations across different classes of DNN models.

Revisiting sparse mask mismatch for FLASH. As demonstrated in Figs 15, the sparse mask mismatch in the case of JMWST significantly reduces, helping the mask train in a convergent way, significantly faster than that in NST.

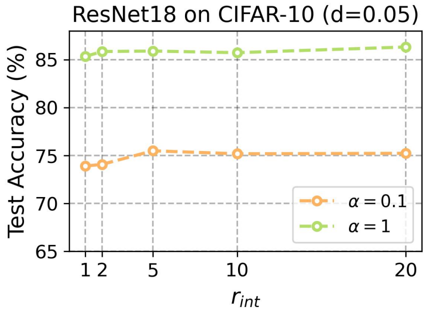

Figure 12: Test accuracy vs. mask update interval round.

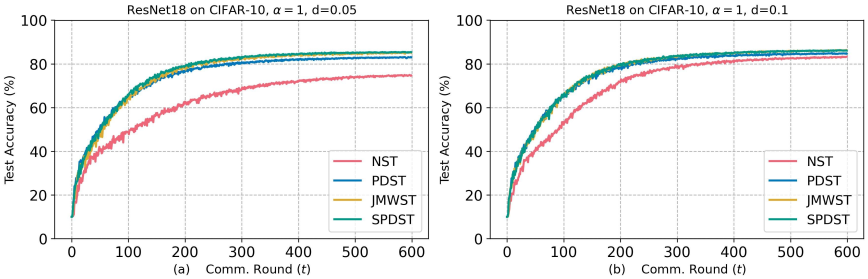

Figure 13: Performance of proposed algorithms vs. comm. rounds on CIFAR-10 dataset for (a) $d = 0.05$ (b) $d = 0.1$.

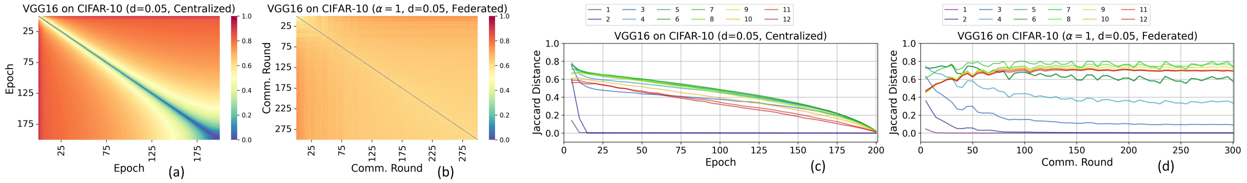

Figure 14: (a)-(b) Sparse mask mismatch (SM) for VGG16 in (a) centralized and (b) FL settings with NST. (c)-(d) Layer-wise SM vs. training epochs (rounds) for VGG16 in (c) centralized and (d) FL settings, respectively, with NST.

Fig. 16 shows the layer-wise SM for the centralized trained model (Fig. 16a) and FL trained model with sparsity (Fig. 16b-c). In particular, the SM at the later layer can significantly reduce in the case of JMWST compared to NST, further demonstrating the convergence ability even at the later layers.

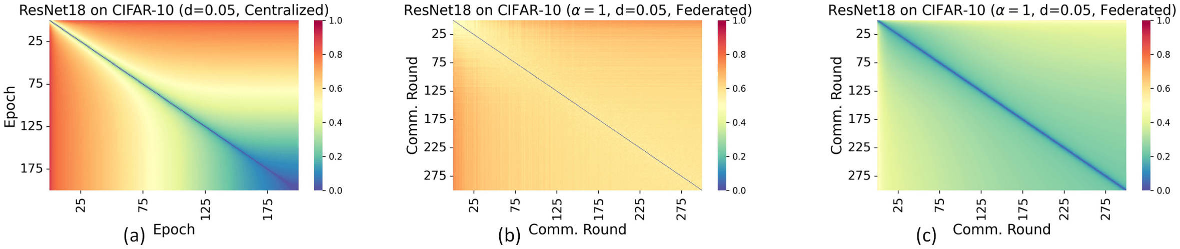

Figure 15: Sparse mask mismatch (SM) for (a) centralized sparse learning, (b) NST, and (c) JMWST in federated settings.

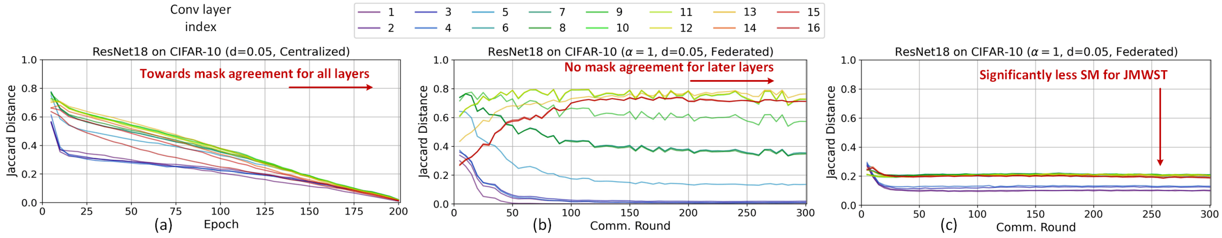

Figure 16: Layer-wise sparse mask mismatch (SM) vs. training epochs (rounds) plot for (a) centralized and (b) FL with NST, and (c) FL with JMWST.

B.6 Sparse mask mismatch as a function of d.

To understand the relation of SM with d, we performed the baseline sparse training (NST) with ResNet18 on CIFAR-10 for three different target densities, 0.05, 0.25, 0.5. As shown in Fig. 17, the SM tends to reduce for higher density. In particular, Fig. 17(d) shows the SM for CONV layer 16 (a later layer) after round 200. The SM reduces by 1.53× for $d = 0.5$ than that with $d = 0.05$, strengthening our general observation that SM becomes prominent as the density decreases.

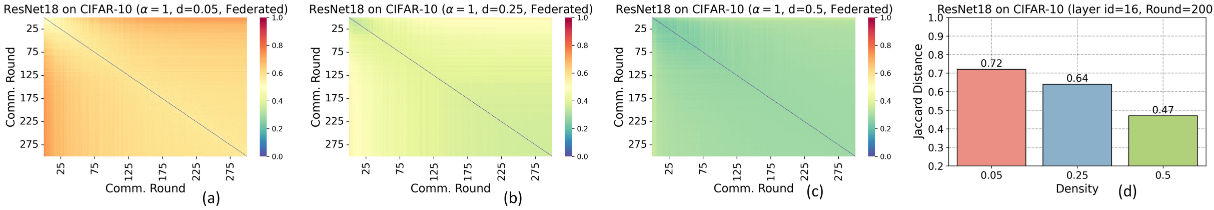

Figure 17: (a-c) SM for FL settings for three different d of 0.05, 0.25, and 0.5, respectively. (d) Comparison of Jaccard distance values for the 16^{th} CONV layer of ResNet18 after round 200 for different ds.

B.7 Sparse mask mismatch as a function of the number of clients.

To understand the relation of SM with the number of total clients, we performed the baseline sparse training (NST) with ResNet18 on CIFAR-10 for 50 and 200 clients, respectively. As shown in Fig. 18, the SM concern persists, irrespective of the number of clients. This strengthens the generality of our observations over the total number of clients.

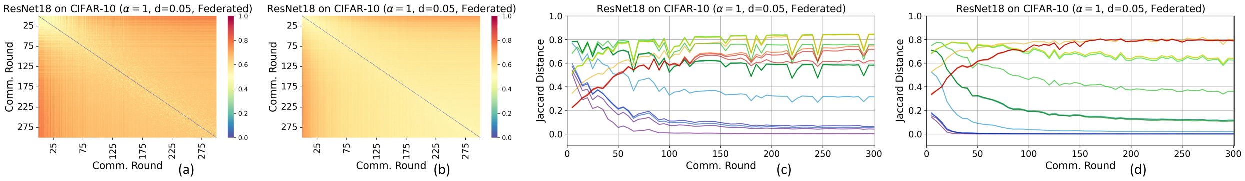

Figure 18: (a-b) SM for FL settings for (a) 50 and (b) 200 clients. (c-d) Layer-wise SM vs. training rounds for (c) 50 and (d) 200 clients.

B.8 Discussion on compute benefits at the edge.

To extract FLOPs benefits for irregular pruning in FLASH, we assume that the compute energy for the sparse network can be avoided via the means of clock-gating (Yang & Kim, 2018) of the zero-valued weights. Moreover, there has been recent development of sparsity-friendly DNN accelerators (Qin et al., 2020) that can efficiently reduce the compute cost by a significant margin. Such accelerators can leverage the yielded sparse FL models to deploy at compute-constrained edges.

B.9 FLOPs vs. communication cost for different density budgets.

To reach a target accuracy value, we now plot the FLOPs to uplink communication cost for different density budgets in Fig. 19.

B.10 Clarification on Sparse Training vs. Sparse Updates.

Here, we want to emphasize that our framework differs from the method proposed for sparsifying the updates such as top-K. In particular, in algorithms that try to sparsify the updates, the clients need to do a

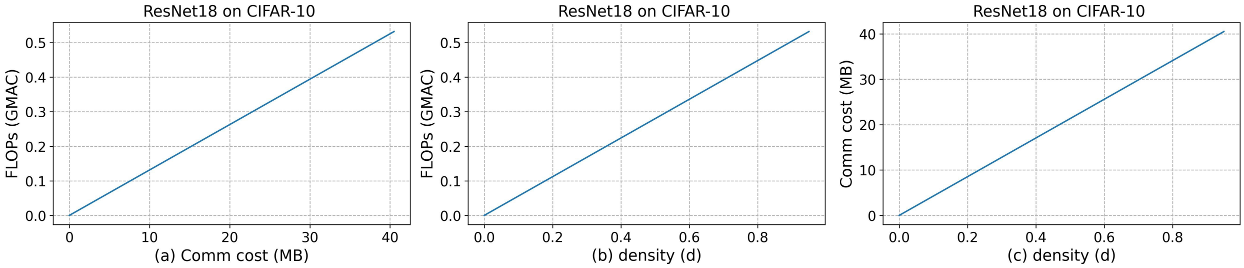

Figure 19: Computation and Communication relation with (a) each other (b, c) with different density levels for SPDST algorithm.

dense gradient update, costing higher computation and potential communication overhead. Our framework, specifically SPFST, on the contrary, ensures only k weights are updated to be non-zero during each round for each client, allowing us to yield the lucrative benefits of sparse gradient computation. Moreover, it ensures each client sends and receives only k weights to and from the server at the end and beginning of each round. Finally, in every round of the top-k algorithm, clients ignore the weights not in the top-k, potentially causing *wasted* computation and performance degradation. However, in SPDST, such *wasted* computations are avoided since only a fixed fraction of weights are trained.

C Computation saving for FLASH.

Employing sparse learning in FL helps participating clients reduce communication and compute costs (FLOPs) for training. Without the loss of generality, we now evaluate the convolutional layer training FLOPs for FLASH and demonstrate the relation of parameter density d with the reduction in FLOPs and communication cost.

The training FLOPs for a layer l (F^l_{layer}) can be partitioned into forward operation FLOPs (F^l_{fwd}), backward input ($F^l_{back\_in}$) and weight gradient ($F^l_{back\_wt}$) compute FLOPs. With the assumption of no-compute cost associated with the zero-valued weights via zero-gating logic (Kundu et al., 2021a), the F^l_{layer} for FLASH with parameter density d ($d << 1.0$) is

$$F^l_{layer} = d \times [Fu^l_{fwd} + Fu^l_{back\_in}] + s_a \times Fu^l_{back\_wt} \tag{4}$$

If the zero weights' gradients flow is computed for mask learning, then F_{back_wt} can't leverage the advantage of low parameter density. Thus gradients are dense in JMWST, and F_{back_wt} is the same as that in dense computation. However, for SPDST or JMWST with $r_{int} > 1$, zero weights remain zero, allowing us to skip the associated gradient computation safely. This helps extract the benefits of sparsity during all three stages of FLOPs computation. In other words, FLASH can improve communication and compute costs for clients with limited resources.

C.1 Evaluation of communication cost.

Communication cost is associated with transmitting the newly updated weight (or gradients) from client to server or vice versa. The communication reduction is achieved by making the weight matrices sparse. In this way, clients do not need to send the whole matrix; instead, they can only send the value of the non-zero ones. In our experiments, we use the compressed sparse row (CSR) format of the sparse model weights to communicate them between clients and the server. Finally, communication-saving is evaluated by the ratio of full dense model communication cost to sparse model in CSR format.

C.2 Discussion on Support for Hardware-Friendly Sparsity Patterns

Irregular sparsity is often not well-suited for hardware benefits without dedicated architecture or compiler support. However, we can yield computation energy saving with custom zero-gating logic (Kundu et al.,

2020) and compiler support (Liu et al., 2018). As we intended to achieve reduced computation energy and communication cost in FL and as irregular sparsity can yield higher compression than structured/pattern sparsity, we have limited our evaluations to random or irregular sparsity only. Nevertheless, we believe our framework can support more complex and structured pruning, which we briefly explain.

Among the various hardware-friendly sparsity patterns recently proposed $N : M$ sparsity (Zhou et al., 2021) has gained significant attention due to its less strict constraints. For SPDST, post stage 1, sparse mask selection can be easily extended to support the $N : M$ sparsity. In particular, for a layer l, instead of random assignment of $d^l \times k^l$ non-zero mask locations, we can partition the total non-zero elements into G^l groups, where each group will contain $d^l \times k^l / G^l$ non-zero elements. Here G^l is evaluated as k^l/M, M representing the total element size out of which we need to have a certain fraction as non-zero, and k^l represents the total number of weights for that layer. As the masks remain frozen, we ensure such a pattern is maintained throughout the training for each client to extract the benefit. For JMWST, we can adapt this principle in the prune and regrow policy during each client's local training. In Table 11, we now show results with pattern pruning with $N : M$ sparsity for the CIFAR-10 dataset.

Table 11: FLASH with structured sparsity for CIFAR-10 dataset

Data Distribution	**Density**	**Method**	**Acc (%)**
non-IID ($\alpha = 1$)	0.2	SPDST	86.96
non-IID($\alpha = 0.1$)	0.2	SPDST	77.64

D Convergence Analysis

Convergence of FedAvg. To demonstrate convergence with the proposed sparse learning, we take inspiration from (Wang et al., 2020) and assume three assumptions that we later show hold true for sparse FL as well.

Assumption 1 (Smoothness). All clients use Lipchitz smooth local objective functions ($||\nabla F_i(x) - \nabla F_i(y)|| \leq L||x - y||, \forall i \in 1, 2, ..., k$).

Assumption 2 (Bounded dissimilarity). There exists a constant β^2 that bounds the client gradient dissimilarity: $\Sigma_i ||\nabla F_i(x)||^2 \leq ||\Sigma_i \nabla F_i(x)||^2$.

Assumption 3 (Unbiased gradient and bounded variance). The stochastic gradient of each gradient has bounded variance $|| \mathbb{E}_c[||g_i(x|c) - \nabla F_i(x)||^2] \leq \sigma^2, \forall i \in 1, 2, ..., K, \sigma^2 \geq 0$ and is an unbiased estimator for its local gradient: $\mathbb{E}_c[g_i(x|c)] = \nabla F_i(x)$.

Under the above three assumptions, (Wang et al., 2020) successfully showed that "*FedAvg converges to a stationary point of a surrogate objective* $\tilde{F}(x) = \Sigma_{i=1}^{k} F_i(x)$."

Convergence of SPDST. We now show that all the above assumptions (1-3) are valid and derivable for masked updates, as in the case of SPDST. Without the loss of generality, here we assume that each client calculates the full gradient and then zeros out the weights associated with the mask value of zero. Thus, instead of gradient, it sends the masked gradient: $\mathcal{M} \odot \nabla F_i$, where $\mathcal{M}$ is a pre-defined and fixed binary mask for all clients.

Assumption 1 (Smoothness). Modified: $||\mathcal{M} \odot \nabla F_i(x) - \mathcal{M} \odot \nabla F_i(y)|| \leq L||x - y||$.

$$||\mathcal{M} \odot \nabla F_i(x) - \mathcal{M} \odot \nabla F_i(y)|| = ||\mathcal{M} \odot (\nabla F_i(x) - \nabla F_i(y))|| =$$
$$\mathcal{M} \odot ||(\nabla F_i(x) - \nabla F_i(y))|| \leq ||\nabla F_i(x) - \nabla F_i(y)|| \leq L||x - y||$$

Assumption 2 (Bounded dissimilarity). Modified: $\Sigma_i ||\mathcal{M} \odot \nabla F_i(x)||^2 \leq ||\Sigma_i \ \mathcal{M} \odot \nabla F_i(x)||^2$

Similar to FedSpa Huang et al. (2022), we assume that this property is also for masked updates as well.

Assumption 3 (Unbiased gradient and bounded variance). Modified (bounded variance): $|| \mathbb{E}_c[||\mathcal{M} \odot g_i(x|c) - \nabla \odot F_i(x)||^2] \leq \sigma^2, \forall i \in 1, 2, ..., K, \sigma^2 \geq 0$.

$$\mathbb{E}_c[||\mathcal{M} \odot g_i(x|c) - \mathcal{M} \odot \nabla F_i(x)||^2] \leq \mathcal{M} \odot \mathbb{E}_c[||(g_i(x|c)) - \nabla F_i(x)||^2] \leq \sigma^2$$

Modified (unbiased gradient): $\mathbb{E}_c[\mathcal{M} \odot g_i(x|c)] = \mathcal{M} \odot \nabla F_i(x)$.

$$\mathbb{E}_c[\mathcal{M} \odot g_i(x|c)] = \mathcal{M} \odot (\mathbb{E}_c[g_i(x|c)]) = \mathcal{M} \odot \nabla F_i(x).$$

Thus we demonstrate that the above assumptions are still valid for the masked update.

Proof. Considering that all three assumptions proposed by (Wang et al., 2020) hold true for SPDST as well, we can conclude the training converges for SPDST.